Calculation of a scalar-isoscalar hadronic correlator

C. M. Shakin* and Huangsheng Wang
Department of Physics and Center for Nuclear Theory, Brooklyn College of the City University of New York, Brooklyn, New York 11210
(Received 22 March 2001; revised manuscript received 27 June 2001; published 9 October 2001)

In an earlier work we calculated the continuum contribution to the hadronic current correlator for pseudoscalar and scalar-isovector currents. In this work we extend our considerations to the study of a scalar-isoscalar correlator of scalar operators. In this formalism we explore the distribution of $q\bar{q}$ strength as a function of energy. We perform a covariant random-phase approximation calculation of the scalar-isoscalar states using parameters that have been determined in earlier studies of pseudoscalar and vector mesons. The state of lowest energy that we find can be identified with the $f_0(980)$. We find very little $q\bar{q}$ strength for energies less than the energy of the $f_0(980)$. That suggests that the nonlinear sigma model is the model of choice, since there is no low-lying scalar state of $q\bar{q}$ character in our model. [The $f_0(400-1200)$, which now appears in the data tables, may be understood as a ''dynamically generated'' state that appears when one studies $\pi\pi$ scattering. In our analysis it is not a $q\bar{q}$ state. In the Nambu–Jona-Lasinio model, chiral symmetry requires the same interaction strength G_S for scalar and pseudoscalar states. If we wished to obtain a scalar state at about 600 MeV, we would require a major violation of chiral symmetry, such that G_S for scalar states would be about 50% larger than the value determined from our study of the pseudoscalar mesons.] We conclude that, except for certain limited applications that we have described in earlier work, the linear sigma model, which describes a low-energy $q\bar{q}$ state of mass of about 500–600 MeV, does not provide a correct description of the physical spectrum.

DOI: 10.1103/PhysRevD.64.094020 PACS number(s): 12.38.Aw, 12.39.Fe, 14.40.Cs

I. INTRODUCTION

We have developed a generalized Nambu–Jona-Lasinio (NJL) model that includes a covariant model of confinement. Using this model we are able to calculate meson spectra up to energies in the 2–3 GeV range [1,2]. One interesting application of the model is the calculation of hadronic current correlation functions. In a previous work we calculated such functions for pseudoscalar and scalar-isovector currents [3]. We were also reasonably successful in reproducing the decay constants of the $a_0(980)$, $a_0(1450)$, and $K_0^*(1430)$ [4] that were obtained by Maltman using QCD sum rule techniques and other methods [5,6].

In this work we wish to study a scalar-isoscalar correlator of the scalars $\bar{q}(x)q(x)$ and $\bar{q}(0)q(0)$. While this calculation has some intrinsic interest, we are motivated to study this correlator because it provides a rather direct measure of the distribution of $q\bar{q}$ strength over a broad range of energies. In this fashion we can study the relative utility of the linear and nonlinear sigma models [7].

It is well known that the NJL model without confinement places the chiral partner of the pion at an energy close to $2m_q$ where m_q is the constituent quark mass of the up or down quark. As we will see, our generalized NJL model, which includes a model of confinement, places the lowest $q\bar{q}$ state at about 1 GeV in energy where it can be identified with the $f_0(980)$. The Lagrangian of our model is

$$\mathcal{L}=\bar{q}(i\partial\!\!\!/-m^0)q+\frac{G_S}{2}\sum_{i=0}^{8}[(\bar{q}\lambda^i q)^2+(\bar{q}i\gamma_5\lambda^i q)^2]$$
$$-\frac{G_V}{2}\sum_{i=0}^{8}[(\bar{q}\gamma^\mu\lambda^i q)^2+(\bar{q}\gamma^\mu\gamma_5\lambda^i q)^2]$$
$$+\frac{G_D}{2}\{\det[\bar{q}(1+\gamma_5)q]+\det[\bar{q}(1-\gamma_5)q]\}$$
$$+\mathcal{L}_{\rm tensor}+\mathcal{L}_{\rm conf}. \tag{1.1}$$

Here, the fourth term is the 't Hooft interaction, $\mathcal{L}_{\rm tensor}$ denotes interactions added to study tensor mesons, and $\mathcal{L}_{\rm conf}$ denotes our model of Lorentz-vector confinement. In Eq. (1.1) m^0 is the current quark mass matrix $m^0=\mathrm{diag}(m_u^0,m_d^0,m_s^0)$, the λ_i $(i=1,...,8)$ are the Gell-Mann matrices, and $\lambda_0=\sqrt{2/3}\,1$, with 1 being the unit matrix in flavor space.

We remark that our calculation of the scalar-isoscalar states may be considered as essentially parameter-free, since the parameters of our NJL model were fixed in a study of pseudoscalar and vector mesons. It is useful to refer to the review of Hatsuda and Kunihiro [8] to obtain the values of the interaction for various mesons in the presence of the 't Hooft interaction. For example, our recent study of the η mesons required the values of the singlet and octet coupling constants

$$G_{00}^P=G_S-\frac{2}{3}(\alpha+\beta+\gamma)\frac{G_D}{2} \tag{1.2}$$

*Email address: casbc@cunyvm.cuny.edu

 ©2001 The American Physical Society

and

$$G_{88}^{P}=G_S-\frac{1}{3}(\gamma-2\alpha-2\beta)\frac{G_D}{2}. \tag{1.3}$$

(We have put the small and somewhat uncertain value of $G_{08}^{P}=0$.) In Eqs. (1.2) and (1.3), α, β, and γ are the vacuum condensates: $\alpha=\langle\bar{u}u\rangle$, $\beta=\langle\bar{d}d\rangle$, and $\gamma=\langle\bar{s}s\rangle$. We have taken $\alpha=\beta=-(0.248\,\mathrm{GeV})^3$ and $\gamma=-(0.258\,\mathrm{GeV})^3$.

The values needed for the study of the f_0 mesons are [8]

$$G_{00}^{S}=G_S+\frac{2}{3}(\alpha+\beta+\gamma)\frac{G_D}{2} \tag{1.4}$$

and

$$G_{88}^{S}=G_S+\frac{1}{3}(\gamma-2\alpha-2\beta)\frac{G_D}{2}. \tag{1.5}$$

In a recent systematic study of the $\eta(547)$ and $\eta'(958)$ and their radial excitations [9], we found $G_{88}^{P}=12.46$ and $G_{00}^{P}=8.60\ \mathrm{GeV}^{-2}$, from which we infer $G_S=11.24$ and $G_D=-166.4\ \mathrm{GeV}^{-5}$. Therefore, for our study of the f_0 mesons, we obtain the values $G_{00}^{S}=13.87$ and $G_{88}^{S}=10.02\ \mathrm{GeV}^{-2}$ when using Eqs. (1.4) and (1.5). The parameter $G_V=12.46\ \mathrm{GeV}^{-2}$ was determined in a study of the vector mesons [1]. (That parameter influences the properties of the pseudoscalar mesons when we take pseudoscalar–axial-vector mixing into account.) The value of the strange quark mass was found by fitting the mass of the $\phi(1020)$ meson after the confining interaction parameter was fitted by studying the radial excitations of the ρ and ω mesons.

Inspection of the Lagrangian of Eq. (1.1) shows that it is chiral symmetry that allows us to specify the interaction for the scalar states by fixing G_S in a study of the pseudoscalar states. The difference between G_{88} and G_{00} is proportional to the strength of the 't Hooft interaction G_D. That interaction is important in the study of the η and f_0 mesons, since such studies involve singlet-octet mixing.

The organization of our work is as follows. In Sec. II we review our model of confinement and define various vertex functions. We discuss our choice of Lorentz-vector confinement and the approximations made in our calculations, the most important being the neglect of any pair currents generated by the confining interaction. In Sec. II we also introduce various vacuum polarization integrals of the NJL model. We make use of these expressions when providing a simple diagrammatic derivation of random-phase approximation (RPA) equations for the study of the f_0 mesons. (The diagrammatic analysis is significantly simpler than the usual derivation that involves construction of the commutator of quark-antiquark operators with the Hamiltonian and the linearization of the equations of motion [10].) In Sec. III we present the equations of the random-phase approximation that we use to calculate the properties of the f_0 mesons. In Sec. IV we discuss the normalization of our wave functions and the calculation of decay constants of these mesons. Section V is devoted to the presentation of some numerical results. In Sec. VI we define and calculate a hadronic correlator for scalar-isoscalar states. Finally, Sec. VII contains some further discussion and conclusions.

II. CONFINEMENT POTENTIAL AND VERTEX FUNCTIONS

There are two important approximations made in our analysis which are related to our treatment of confinement. Our confinement model is meant to describe the interaction due to the presence of a chromoelectric flux tube between the quark and the antiquark. We have found it necessary to neglect the generation of pair currents by the confining interaction. As we will see, two important vertex functions $\Gamma^{+-}(P,k)$ and $\Gamma^{-+}(P,k)$ appear in our formalism. In the past we have derived coupled equations satisfied by these functions. However, in our study of pseudoscalar mesons we found that the coupling terms were so large as to preclude meaningful solutions of the coupled equations, while the uncoupled equations were easily solved and gave excellent results when the corresponding vertex functions were used in the calculation of meson spectra. (The coupled equations for Γ_P^{+-} and Γ_P^{-+} for pseudoscalar mesons were presented in Appendix C of Ref. [11]. There it may be seen that the coupling terms are very much larger than the terms that connect Γ^{+-} and Γ^{-+} to themselves. It is the coupling terms that give rise to the pair currents mentioned above.) We have solved the uncoupled equations for the vertex functions in the meson rest frame. Once the various vertex functions are calculated, the formalism can be made covariant, as noted later in this section. [See Eqs. (2.15)–(2.17).]

The other important approximation we have made is to use constant values for the constituent quark masses. In our earlier work [12], we solved the Bethe-Salpeter equation in conjunction with the Schwinger-Dyson equation in Euclidean space. It was then easy to show that Goldstone's theorem was satisfied, with the pion as the Goldstone boson. That procedure led to some momentum dependence of the constituent quark mass in Euclidean space. It is unclear as to how to carry out such a calculation in Minkowski space. There are also some questions that arise when attempting to derive a Schwinger-Dyson equation, since our model of confinement is based upon the potential generated by the chromoelectric flux tube between the quark and the antiquark. The Schwinger-Dyson equation refers to the properties of a single quark. It is rather difficult to imagine the quark emitting and absorbing the flux tube in analogy with the electron self-energy calculation in QED. Given these difficulties, we have proceeded with a phenomenological scheme in which we choose constants for the constituent quark masses. These constant values may be thought of as momentum-space averages of the running quark mass values which are presently unknown.

It is of some interest to note that the problem of large pair-current effects may be avoided if we use the confining interaction used in Ref. [12] which has a "$V-A$" form. That is, we substract from our model of vector confinement the expression for axial-vector confinement. In that case we can readily solve the equations for the vertex function without

making any approximations with respect to pair-current effects. However, we have not as yet developed a Minkowski-space phenomenology for the interaction introduced in Ref. [12]. Therefore, in the present work we will continue to use Lorentz-vector confinement and solve the uncoupled equations for the vertex functions $\Gamma^{+-}(P,k)$ and $\Gamma^{-+}(P,k)$.

Our model of confinement is based upon the coordinate-space potential $V(r)=\kappa r \exp[-\mu r]$, where μ is a small parameter introduced to facilitate our momentum-space calculations. Note that we do not have absolute confinement in our model. However, the $q\bar{q}$ states in the confining field are readily separated into states inside the potential barrier and scattering states that show little barrier penetration. We have $V_{\max}=\kappa/\mu e$, which for $\kappa=0.055$ GeV^2 and $\mu=0.010$ GeV yields $V_{\max}=2.023$ GeV. Thus, we can find bound states in the interior region of the potential up to $E_{\max}=m_a+m_b+2.023$ GeV for $q\bar{q}$ states with $L=0$. For constituent masses $m_u=0.364$ and $m_s=0.565$ GeV, $E_{\max}=2.751$ GeV if we study $n\bar{n}$ systems and $E_{\max}=2.952$ GeV for $n\bar{s}$ systems with $L=0$. Smaller values of μ may be used if we wish to increase the value of $E_{\max}$. For $\mu=0.010$ GeV, we can find from eight to ten states bound in the confining field when we study scalar-isovector mesons, for example. (Barrier penetration is of no importance in this model.)

The Fourier transform of $V(r)$ is

$$V^C(\vec{k}-\vec{k}')=-8\pi\kappa\left[\frac{1}{[(\vec{k}-\vec{k}')^2+\mu^2]^2}-\frac{4\mu^2}{[(\vec{k}-\vec{k}')^2+\mu^2]^3}\right]. \tag{2.1}$$

The model is made covariant through the use of the four-vectors

$$\hat{k}^\mu=k^\mu-\frac{(k\cdot P)P^\mu}{P^2}, \tag{2.2}$$

and

$$\hat{k}'^\mu=k'^\mu-\frac{(k'\cdot P)P^\mu}{P^2}, \tag{2.3}$$

since in the meson rest frame $(\vec{P}=\vec{0})\hat{k}^\mu-\hat{k}'^\mu=[0,\vec{k}-\vec{k}']$. Thus, we may write

$$V^C(\hat{k}-\hat{k}')=-8\pi\kappa\left[\frac{1}{[-(\hat{k}-\hat{k}')^2+\mu^2]^2}-\frac{4\mu^2}{[-(\hat{k}-\hat{k}')^2+\mu^2]^3}\right]. \tag{2.4}$$

As noted above, in our work we have used a model of Lorentz-vector confinement. Various arguments have been put forth by Szczepaniak and Swanson [13] to justify the use of Lorentz-vector rather than scalar confinement. For example, scalar confinement is generally used in the case of heavy quark systems. In Ref. [13] it is argued that nonperturbative mixing between ordinary and hybrid $q\bar{q}$ states leads to an *effective* scalar confinement model, which hides the underlying Lorentz-vector character of the confining interaction. These authors also point out that vector confinement is the natural choice if one wishes to write a chirally symmetric interaction that allows for spontaneous chiral symmetry breaking in the vacuum and the appearance of Goldstone bosons. It is also noted that scalar confinement does not lead to a stable vacuum state [13].

We use the confining interaction to construct equations for various vertex functions [1,2]. Let us consider the case of the scalar vertex for equal mass quarks. In the meson rest frame we may write

$$\bar{\Gamma}^S(P,K)=1-i\int\frac{d^4k'}{(2k)^4}[\gamma^\rho S(P/2+k')\bar{\Gamma}^S(P,k')\times S(-P/2+k')\gamma_\rho]V^C(\vec{k}-\vec{k}'). \tag{2.5}$$

[See Fig. 1(a) and Eq. (2.19) below.] Here, $\bar{\Gamma}^S(P,k)$ has a matrix structure. The Dirac matrices γ^ρ and γ_ρ appear in Eq. (2.5) because we are using Lorentz-vector confinement. It is useful to introduce functions Γ_S^{+-} and Γ_S^{-+} [1,2]. First, we define the projection operators

$$\Lambda^{(+)}(\vec{k})=\frac{\not{k}+m}{2m} \tag{2.6}$$

and

$$\Lambda^{(-)}(-\vec{k})=\frac{\tilde{\not{k}}+m}{2m}, \tag{2.7}$$

with $k^\mu=[E(\vec{k}),\vec{k}]$ and $\tilde{k}^\mu=[-E(\vec{k}),\vec{k}]$. Note that $\Lambda^{(+)}(\vec{k})+\Lambda^{(-)}(\vec{k})=1$, with $\Lambda^{(-)}(\vec{k})=(-\not{k}+m)/2m$. Then we write (for $\vec{P}=\vec{0}$)

$$\Lambda^{(+)}(\vec{k})\bar{\Gamma}^S(P,k)\Lambda^{(-)}(-\vec{k})=\Gamma_S^{+-}(P,k)\Lambda^{(+)}(\vec{k})\Lambda^{(-)}(-\vec{k}), \tag{2.8}$$

$$\Lambda^{(-)}(-\vec{k})\bar{\Gamma}^S(P,k)\Lambda^{(+)}(\vec{k})=\Gamma_S^{-+}(P,k)\Lambda^{(-)}(-\vec{k})\Lambda^{(+)}(\vec{k}), \tag{2.9}$$

$$\Lambda^{(+)}(\vec{k})\bar{\Gamma}^S(P,k)\Lambda^{(+)}(\vec{k})=\Gamma_S^{++}(P,k)\Lambda^{(+)}(\vec{k}), \tag{2.10}$$

and

$$\Lambda^{(-)}(-\vec{k})\bar{\Gamma}^S(P,k)\Lambda^{(-)}(-\vec{k})=\Gamma_S^{--}(P,k)\Lambda^{(-)}(-\vec{k}). \tag{2.11}$$

As we will see, the use of Eqs. (2.8)–(2.11) makes it particularly simple to neglect pair currents in our formalism. Equations for Γ_S^{+-}, Γ_S^{-+}, Γ_S^{++}, and Γ_S^{--} may be obtained by multiplying Eq. (2.5) from the left and from the right by one of the projection operators in Eqs. (2.6), (2.7) and then taking the trace. In our work we obtained the following *uncoupled* equations for $\Gamma_S^{+-}(P,k)$ and $\Gamma_S^{-+}(P,k)$ in the frame where $\vec{P}=\vec{0}$ [2]:

$$\Gamma_S^{+-}(P^0,k)=1+\frac{1}{(2\pi)^2}\int k'^2dk'[2k'^2k^2V_0^C(k,k') + m^2kk'V_1^C(k,k')]\frac{1}{k^2E^2(\vec{k}')}\frac{\Gamma_S^{+-}(P^0,k')}{P^0-2E(\vec{k}')} \tag{2.12}$$

and

$$\Gamma_S^{-+}(P^0,k)=1-\frac{1}{(2\pi)^2}\int k'^2dk'[2k'^2k^2V_0^C(k,k') + m^2kk'V_1^C(k,k')]\frac{1}{k^2E^2(\vec{E}')}\frac{\Gamma_S^{-+}(P^0,k')}{P^0+2E(\vec{k}')}. \tag{2.13}$$

The calculation of $\Gamma_S^{++}(P^0,k)$ and $\Gamma_S^{--}(P^0,k)$ is described in Ref. [2]. In Eqs. (2.12) and (2.13) $k=|\vec{P}|$ and $k'=|\vec{P}'|$. With $x=\cos\theta$, we have

$$V_l^C(k,k')=\frac{1}{2}\int_{-1}^{1}dx\,P_l(x)V^C(\vec{k}-\vec{k}'), \tag{2.14}$$

where $P_l(x)$ is a Legendre polynomial. This formalism may be used to obtain covariant expressions for the vertex [1,2]. We write

$$\overline{\Gamma}_S(P,k)=a_1(P,k)+\hat{\not{k}}a_2(P,k), \tag{2.15}$$

where $\hat{k}^\mu$ was defined previously in Eq. (2.2). We have

$$\Gamma_S^{+-}(P,k)=a_1(P,k)+ma_2(P,k), \tag{2.16}$$

$$\Gamma_S^{++}(P,k)=a_1(P,k)-\frac{\vec{k}^2}{m}a_2(P,k). \tag{2.17}$$

Note that we can write $a_1(P,k)=a_1(P^2,\sqrt{-\hat{k}^2})$ and $a_2(P,k)=a_2(P^2,\sqrt{-\hat{k}^2})$. The Lorentz invariants a_1 and a_2 may be determined by relating them to the rest frame values of $\Gamma_S^{+-}(P^0,|\vec{k}|)$ and $\Gamma_S^{++}(P^0,|\vec{k}|)$ [1,2]. (The case in which the quark masses are different is discussed in great detail in Ref. [1].) Using this formalism, vacuum polarization diagrams and meson decay amplitudes may be calculated in any Lorentz frame and we have made a number of such calculations.

It is important to note that $\Gamma_S^{+-}(P^0,k)=0$ when $P^0=2E(\vec{k})$. Thus, the ratio $\Gamma_S^{+-}(P^0,k)/[P^0-2E(\vec{k})]$ is finite. It is that feature that leads to real values of the polarization integrals for $P^0>2m_q$.

The vertex functions defined above are represented by the filled triangular region in Fig. 1(a). We may also define vertex functions that are the solutions of the homogeneous equation depicted in Fig. 1(b). The resulting vertex functions and corresponding wave functions describe the $q\overline{q}$ states bound by the confining field V^C.

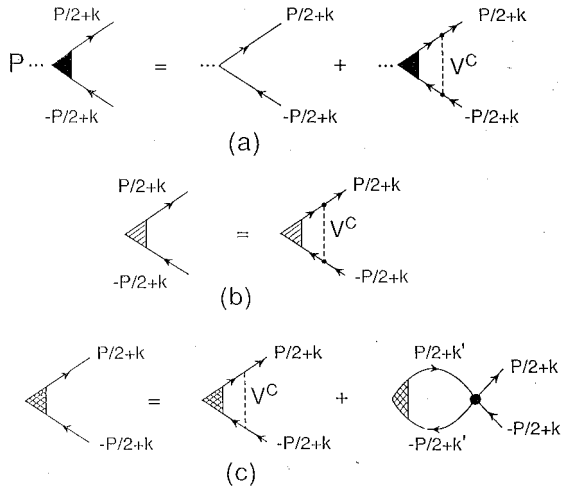

FIG. 1. (a) Schematic representation of the equation for the confinement vertex. Here V^C denotes the confining field [1,2]. (b) The homogeneous version of the equation shown in (a) is represented. (c) A representation of the homogeneous equation for the vertex $\hat{\Gamma}$ that includes the effects of both confinement and the short-range NJL interaction is shown.

In this work we will be mainly interested in the solution of the equation depicted in Fig. 1(c). As may be inferred from the figure, the resulting vertex functions, and corresponding wave functions, describe the bound states that are influenced by *both* the confining field and the short-range NJL interaction. The normalized vertex functions will be denoted by a caret, so that the scalar vertex will be written as $\hat{\Gamma}^S(P,k)$, for example. [See Eqs. (3.21) and (3.22) below.]

The vacuum polarization function seen in Fig. 2(a) is

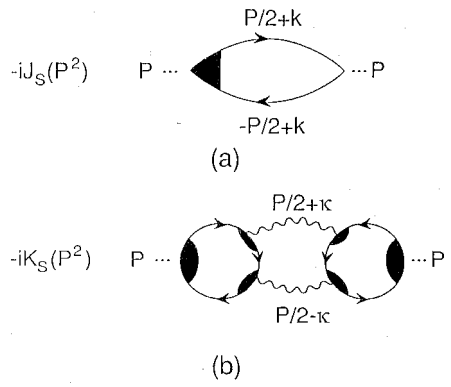

FIG. 2. (a) The diagram serves to define the function $-iJ^s(P^2)$. The triangular filled regions are the vertex functions shown in Fig. 1(a). (b) The diagram represents the function $-iK^s(P^2)$ that describes polarization effects due to coupling to two-meson decay channels. The channels $\pi\pi$, $K\overline{K}$, $\eta\eta$, and $\eta\eta'$ were considered in Ref. [2] and values for $K^S_{\pi\pi}(P^2)$ and $K^S_{K\overline{K}}(P^2)$ were presented there.

given by the integral

$$-iJ^S(P^2)=-2n_C\int\frac{d^4k}{(2\pi)^4}\mathrm{Tr}[iS(P/2+k)\times\overline{\Gamma}^S(P,k)iS(-p/2+k)], \tag{2.18}$$

when we study scalar mesons. Here $n_C=3$ is the number of colors and the factor 2 arises from the flavor trace. In Eq. (2.18) $S(P/2+k)$ and $S(-P/2+k)$ are propagators for constituent quarks of mass m, $S(p)=[\not p-m+i\eta]^{-1}$. In evaluating Eq. (2.18) it is useful to use a representation defined in the meson rest frame ($\vec{P}=\vec{0}$):

$$S(P/2+k)=\frac{m}{E(k)}\left[\frac{\Lambda^{(+)}(\vec{k})}{P^0/2+k^0-E(\vec{k})+i\eta}-\frac{\Lambda^{(-)}(-\vec{k})}{P^0/2+k^0+E(\vec{k})-i\eta}\right], \tag{2.19}$$

etc. When the projection operators $\Lambda^{(+)}(\vec{k})$ and $\Lambda^{(-)}(-\vec{k})$ appear on either side of $\overline{\Gamma}^S(P,k)$ they give rise to the functions $\Gamma_S^{-+}(P,k)$ and $\Gamma_S^{+-}(P,k)$ defined in Eqs. (2.8) and (2.9). In that manner, after integrating in the complex k^0 plane, we obtain

$$J^S(P^2)=-4n_C\int\frac{d^3k}{(2\pi)^3}\left[\frac{\vec{k}^2}{E^2(\vec{k})}\right]e^{-\vec{k}^2/\alpha^2}\left[\frac{\Gamma_S^{+-}(P^0,|\vec{k}|)}{P^0-2E(\vec{k})}-\frac{\Gamma_S^{-+}(-P^0,|\vec{k}|)}{P^0+2E(\vec{k})}\right]. \tag{2.20}$$

In Eq. (2.20) we have included a Gaussian regulator $\exp[-\vec{k}^2/\alpha^2]$, which can be written in a covariant form using the four-vector $\hat{k}^\mu$ of Eq. (2.2). (In our earlier work, we used $\alpha=0.605\,\mathrm{GeV}$ and we will use that value here.)

It is important to note that from Eqs. (2.12) and (2.13) we have

$$\Gamma_S^{-+}(-P^0,|\vec{k}|)=\Gamma_S^{+-}(P^0,|\vec{k}|), \tag{2.21}$$

so that Eq. (2.20) becomes

$$J^s(P^2)=-4n_C\int\frac{d^3k}{(2\pi)^3}\left(\frac{\vec{k}^2}{E^2(\vec{k})}\right)e^{-\vec{k}/\alpha^2}\Gamma_S^{+-}(P^0,|\vec{k}|)\times\left[\frac{1}{P^0-2E(\vec{k})}-\frac{1}{P^0+2E(\vec{k})}\right]. \tag{2.22}$$

In some of our calculations we have kept only the first term in the square bracket of Eq. (2.22). That procedure defines the Tamm-Dancoff approximation, while the complete expression defines the RPA.

For further analysis it is useful to define two auxiliary functions that are expressed in terms of the normalized vertex functions $\hat{\Gamma}(P,k)$:

$$\tilde{J}^S_{n\overline{n}}(P^2)=-4n_C\int\frac{d^3k}{(2\pi)^3}\left[\frac{\vec{k}^2}{E_n^2(\vec{k})}\right]\hat{\Gamma}^{+-}_{n\overline{n}}(P^0,|\vec{k}|)\times\left[\frac{1}{P^0-2E_n(\vec{k})}-\frac{1}{P^0+2E_n(\vec{k})}\right] \tag{2.23}$$

and

$$\tilde{J}^S_{s\overline{s}}(P^2)=-4n_C\int\frac{d^3k}{(2\pi)^3}\left[\frac{\vec{k}^2}{E_s^2(\vec{k})}\right]\hat{\Gamma}^{+-}_{s\overline{s}}(P^0,|\vec{k}|)\times\left[\frac{1}{P^0-2E_s(\vec{k})}-\frac{1}{P^0+2E_s(\vec{k})}\right]. \tag{2.24}$$

Here, $n\overline{n}=(1/\sqrt{2})[u\overline{u}+d\overline{d}]$, so that $\tilde{J}^S(P^2)$ is defined separately for the up (or down) quarks and the strange quark. These functions are useful in a diagrammatic derivation of RPA equations made using Fig. 1(c).

In Fig. 2(b) we give a pictorial representation of a vacuum polarization function $-iK_S(P^2)$ that describes the influence of the coupling to the two-meson continuum. That coupling is calculated at one-loop order, with the result that $K_S(P^2)$ is of order 1, while $J_S(P^2)$ is of order n_C. We will discuss the role of $K_S(P^2)$ at a later point in this work. At this point, we note that for the f_0 mesons the relevant two-meson decay channels are $\pi\pi$, $K\overline{K}$, $\eta\eta$, $\eta\eta'$, etc.

III. RANDOM-PHASE APPROXIMATION FOR SCALAR-ISOSCALAR MESONS

We may use Eqs. (2.12) and (2.13) to obtain equations that determine the bound states in the confining field considered in isolation. Let us define the wave function solutions of the homogeneous equations for the confining interaction,

$$\phi^+_{c,n\overline{n}}(P_i^0,k)=\frac{\Gamma_S^{+-}(P_i^0,k)}{P_i^0-2E_n(k)} \tag{3.1}$$

and

$$\phi^-_{c,n\overline{n}}(P_i^0,k)=-\frac{\Gamma_S^{-+}(P_i^0,k)}{P_i^0+2E_n(k)}, \tag{3.2}$$

with similar definitions of $\phi^+_{c,s\overline{s}}(k)$ and $\phi^-_{c,s\overline{s}}(k)$. Here, P_i^0 is the eigenvalue for the bound state labeled by the index c.

Using Eqs. (2.12) and (2.13), we have

$$[P^0-2E_n(k)]\phi^+_{c,nn^-}(k)=\frac{1}{(2\pi)^2}\int k'^2dk' \times[2k'^2k^2V_0^C(k,k') +m^2kk'V_1^C(k,k')] \times\frac{1}{k^2E^2(k')}\phi^+_{c,nn^-}(k') \quad (3.3)$$

and

$$[P^0+2E_n(k)]\phi^-_{c,nn^-}(k) =-\frac{1}{(2\pi)^2}\int k'^2dk'[2k'^2k^2V_0^C(k,k') +m^2kk'V_1^C(k,k')]\frac{1}{k^2E^2(k')}\phi^-_{c,nn^-}\phi^-_{c,nn^-}(k'). \quad (3.4)$$

There are two other similar equations for $\phi^+_{c,ss^-}(k)$ and $\phi^-_{c,ss^-}(k)$. Here, we have suppressed the index i. We remark that these equations do not require regularization for large k or k'.

We have now obtained equations that allow us to solve for the wave functions bound in the confining field. [See Fig. 1(b).] To proceed we need to add the terms that allow us to solve for the wave functions associated with the vertex functions of Fig. 1(c), $\hat{\Gamma}(P,k)$. For the moment, we may neglect the confining interaction and consider only the NJL interaction. The use of the auxiliary functions $\tilde{J}_S(P^2)$ allows us to provide an elementary derivation of a covariant version of the RPA for the study of meson states of $q\bar{q}$ character. (We will introduce the NJL regulator at a later point.) We begin by using an $n\bar{n}$-$s\bar{s}$ representation. Thus, we may write equations for the vertex functions $\Gamma_{nn^-}(k)$ and $\Gamma_{ss^-}(k)$:

$$\Gamma_{nn^-}(k)=\tilde{J}_{nn^-}(P^2)G_{nn^-,nn^-}+\tilde{J}_{ss^-}(P^2)G_{ss^-,nn^-} \quad (3.5)$$

and

$$\Gamma_{ss^-}(k)=\tilde{J}_{ss^-}(P^2)G_{ss^-,ss^-}+\tilde{J}_{nn^-}(P^2)G_{nn^-,ss^-}. \quad (3.6)$$

In writing Eq. (3.5) we have removed a common factor of λ_{nn^-} [see Eq. (3.23)] and in the case of Eq. (3.6) we have removed a common factor of λ_{ss^-}. Also, since we are working with scalar-isoscalar states, we have a unit matrix in the Dirac space that is not written explicitly in Eqs. (3.5) and (3.6). Let us define

$$\Lambda_n^{(+)}(\vec{k})\Gamma_{nn^-}(P^0,k)\Lambda_n^{(-)}(-\vec{k}) =\Gamma^{+-}_{nn^-}(P^0,k)\Lambda_n^{(+)}(\vec{k})\Lambda_n^{(-)}(-\vec{k}) \quad (3.7)$$

and

$$\Lambda_n^{(-)}(\vec{k})\Gamma_{nn^-}(P^0,k)\Lambda_n^{(+)}(\vec{k}) =\Gamma^{-+}_{nn^-}(P^0,k)\Lambda_n^{(-)}(-\vec{k})\Lambda_n^{(+)}(\vec{k}). \quad (3.8)$$

Similar definitions are made for $\Gamma^{+-}_{ss^-}(P^0,k)$ and $\Gamma^{-+}_{ss^-}(P^0,k)$. It is then useful to define bound-state wave functions

$$\phi^+_{nn^-}(k)=\frac{\Gamma^{+-}_{nn^-}(P_0,k)}{P^0-2E_n(\vec{k})}, \quad (3.9)$$

$$\phi^-_{nn^-}(k)=-\frac{\Gamma^{+-}_{nn^-}(P_0,k)}{P^0+2E_n(\vec{k})}, \quad (3.10)$$

$$\phi^+_{ss^-}(k)=\frac{\Gamma^{+-}_{ss^-}(P_0,k)}{P^0-2E_s(\vec{k})}, \quad (3.11)$$

and

$$\phi^-_{ss^-}(k)=-\frac{\Gamma^{+-}_{ss^-}(P_0,k)}{P^0+2E_s(\vec{k})}. \quad (3.12)$$

We recall that $\Gamma^{-+}_{nn^-}(-P^0,k)=\Gamma^{+-}_{nn^-}(P^0,k)$, etc.

We may multiply Eq. (3.5) on the left by $\Lambda_n^{(+)}(\vec{k})$ and on the right by $\Lambda_n^{(-)}(-\vec{k})$ and form the trace to obtain an equation for $\Gamma^{+-}_{nn^-}(k)$. If we multiply from the left by $\Lambda^{(-)}(-\overline{k})$ and on the right by $\Lambda_n^{(+)}(\overline{k})$, we obtain an equation for $\Gamma^{-+}_{nn^-}(-P^0,k)=\Gamma^{+-}_{nn^-}(P^0,k)$. Using Eqs. (3.9)–(3.12), we find

$$[P^0-2E_n(k)]\phi^+_{nn^-}(k)=\int dk'H_{nn^-}(k,k')G_{nn^-,nn^-}[\phi^+_{nn^-}(k') +\phi^-_{nn^-}(k')] +\int dk'H_{ss^-}(k,k')G_{ss^-,nn^-}[\phi^+_{ss^-}(k') +\phi^-_{ss^-}(k')] +\int dk'V^C_{nn^-}(k,k')\phi^+_{nn^-}(k'), \quad (3.13)$$

$$[P^0+2E_n(k)]\phi^-_{nn^-}(k)=-\int dk'H_{nn^-}(k,k')G_{nn^-,nn^-}[\phi^+_{nn^-}(k') +\phi^-_{nn^-}(k')] -\int dk'H_{ss^-}(k,k')G_{ss^-,nn^-} \times[\phi^+_{ss,^-}(k')+\phi^-_{ss^-}(k')] -\int dk'V^C_{nn^-}(k,k')\phi^-_{nn^-}(k'), \quad (3.14)$$

and two similar equations for $\phi^{+}_{s\bar{s}}(k)$ and $\phi^{-}_{s\bar{s}}(k)$. Here we have used Eqs. (3.3) and (3.4) so as to include the confining interaction in Eqs. (3.13) and (3.14). Note that the confining interaction only couples $\phi^{+}_{n\bar{n}}(k)$ to itself and $\phi^{-}_{n\bar{n}}(k)$ to itself, etc. This feature is related to the neglect of pair currents in the meson rest frame.

It is useful to symmetrize the interaction by introducing the functions

$$\bar{\phi}^{+}_{n\bar{n}}(k)=\frac{k^2}{E_n(k)}\phi^{+}_{n\bar{n}}(k), \tag{3.15}$$

$$\bar{\phi}^{-}_{n\bar{n}}(k)=\frac{k^2}{E_n(k)}\phi^{-}_{n\bar{n}}(k), \tag{3.16}$$

$$\bar{\phi}^{+}_{s\bar{s}}(k)=\frac{k^2}{E_s(k)}\phi^{+}_{s\bar{s}}(k), \tag{3.17}$$

and

$$\bar{\phi}^{-}_{s\bar{s}}(k)=\frac{k^2}{E_s(k)}\phi^{-}_{s\bar{s}}(k). \tag{3.18}$$

The functions $\bar{\phi}^{+}_{n\bar{n}}(k)$, $\bar{\phi}^{-}_{n\bar{n}}(k)$, $\bar{\phi}^{+}_{s\bar{s}}(k)$, and $\bar{\phi}^{-}_{s\bar{s}}(k)$ satisfy equations of the form of Eqs. (3.13) and (3.14), etc., with $H_{n\bar{n}}(k,k')$, $H_{s\bar{s}}(k,k')$, $V^{C}_{n\bar{n}}(k,k')$, and $V^{C}_{s\bar{s}}(k,k')$ replaced by $\bar{H}_{n\bar{n}}(k,k')$, $\bar{H}_{s\bar{s}}(k,k')$, $\bar{V}^{C}_{n\bar{n}}(k,k')$, and $\bar{V}^{C}_{s\bar{s}}(k,k')$. The form of the latter interactions is given in the Appendix.

The RPA equations are regulated by the replacements

$$G_{00}\rightarrow e^{-k^2/2\alpha^2}G_{00}e^{-k^{t2}/2\alpha^2} \tag{3.19}$$

and

$$G_{88}\rightarrow e^{-k^2/2\alpha^2}G_{88}e^{-k^{t2}/2\alpha^2}. \tag{3.20}$$

(We recall that the confining interaction does not require regulation.) We also see that the replacements of Eqs. (3.19) and (3.20) correspond to regulating the vacuum polarization function $J_S(P^2)$ with a Gaussian factor $\exp[-k^2/\alpha^2]$. [See Eqs. (2.20) and (2.22).]

We may normalize these wave function amplitudes by requiring that the meson contain a single quark. (See Sec. IV.) The normalized functions may be denoted as $\phi^{+}_{n\bar{n},N}(k), \phi^{-}_{n\bar{n},N}(k)$, etc. These are related to normalized vertex functions $\hat{\Gamma}_{n\bar{n}}(P^0,k)$ and $\hat{\Gamma}_{s\bar{s}}(P^0,k)$:

$$\phi^{+}_{n\bar{n},N}(k)=\frac{k^2}{E_n(k)}\frac{\hat{\Gamma}^{+-}_{n\bar{n}}(P^0,k)}{P^0-2E_n(k)}, \tag{3.21}$$

$$\phi^{-}_{n\bar{n},N}(k)=-\frac{k^2}{E_n(k)}\frac{\hat{\Gamma}^{+-}_{n\bar{n}}(P^0,k)}{P^0+2E_n(k)}, \tag{3.22}$$

etc.

It is often useful to solve our RPA equations by passing from the $n\bar{n}$-$s\bar{s}$ representation to a singlet-octet representation. We note that

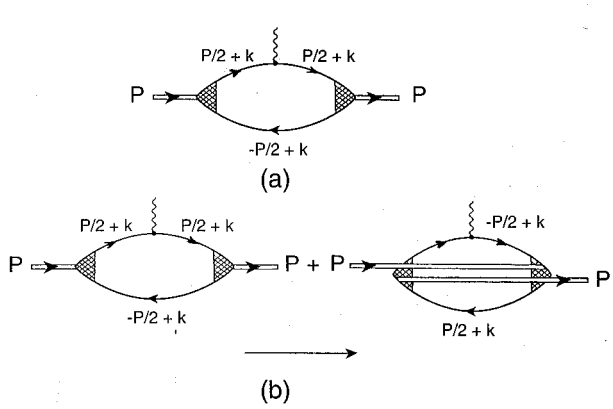

FIG. 3. (a) The normalization constant of the meson wave function is obtained by requiring that the meson contain a single quark. The wavy line serves to introduce the quark number operator. The cross-hatched area denotes the vertex that includes both the effects of confinement and the short-range NJL interaction. (b) The figure shows the Goldstone diagrams that result when one completes the integral over k^0 implied in (a) above. Here, time increases to the right. The first and second diagrams introduce the wave functions with plus and minus superscripts, respectively.

$$\begin{pmatrix}\lambda_{n\bar{n}}\\ \lambda_{s\bar{s}}\end{pmatrix}=M\begin{pmatrix}\lambda_g/\sqrt{2}\\ \lambda_0/\sqrt{2}\end{pmatrix} \tag{3.23}$$

with

$$M=\frac{1}{\sqrt{3}}\begin{pmatrix}1 & \sqrt{2}\\ -\sqrt{2} & 1\end{pmatrix}. \tag{3.24}$$

We also note that

$$\begin{pmatrix}G_{88} & G_{80}\\ G_{08} & G_{00}\end{pmatrix}=M^{-1}\begin{pmatrix}G_{n\bar{n},n\bar{n}} & G_{n\bar{n},s\bar{s}}\\ G_{s\bar{s},n\bar{n}} & G_{s\bar{s},s\bar{s}}\end{pmatrix}M \tag{3.25}$$

and

$$\begin{pmatrix}H_{88} & H_{80}\\ H_{08} & H_{00}\end{pmatrix}=M^{-1}\begin{pmatrix}H_{n\bar{n}} & 0\\ 0 & H_{s\bar{s}}\end{pmatrix}M. \tag{3.26}$$

IV. CALCULATION OF NORMALIZED WAVE FUNCTIONS AND MESON DECAY CONSTANTS

The calculation of the normalization factor that allows us to define normalized wave functions,

$$\phi^{+}_{n\bar{n},N}(k)=\sqrt{N_i}\phi^{+}_{n\bar{n}}(k), \tag{4.1}$$

$$\bar{\phi}^{+}_{n\bar{n},N}(k)=\sqrt{N_i}\bar{\phi}^{+}_{n\bar{n}}(k), \tag{4.2}$$

etc., may be made with reference to Fig. 3. We require that the meson contains a single quark, with the result that

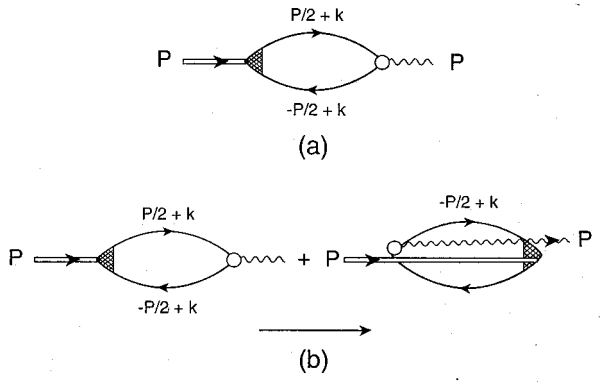

FIG. 4. (a) The calculation of the meson decay constant requires the calculation of the Feynman diagram shown. Here the open circle represents the operator $\bar{q}(0)q(0)$. (b) The Goldstone diagrams that appear when the integral over k^0 implied in (a) is completed. The first and second diagrams introduce the wave functions with plus and minus superscripts, respectively. Here, time increases as one moves to the right in the diagram.

$$\frac{1}{N_i}=\frac{2n_C}{\pi^2}\left(\frac{1}{2M_i}\right)\int k^2dk\left[\frac{k}{E_u(k)}\right]^2\{|\phi^+_{n\bar{n}}(k)|^2-|\phi^-_{n\bar{n}}(k)|^2\}$$
$$+\frac{2n_C}{\pi^2}\left(\frac{1}{2M_i}\right)\int k^2dk\left[\frac{k}{E_s(k)}\right]^2\{|\phi^+_{s\bar{s}}(k)|^2-|\phi^-_{s\bar{s}}(k)|^2\}. \tag{4.3}$$

In Eq. (4.3) the wave functions are obtained from those given by the computer code that solves the symmetrized equations

$$\phi^+_{n\bar{n}}(k)=[E_u(k)/k^2]\bar{\phi}^+_{n\bar{n}}(k), \tag{4.4}$$

etc. [We recall that the wave functions on the right-hand side of Eq. (4.4) satisfy the symmetrized RPA equations. See the remarks made after Eq. (3.18).]

To calculate the decay constant we consider the diagram of Fig. 4. There, the cross-hatched region refers to $\hat{\Gamma}(P,k)$, while the open circle represents the scalar operator $\bar{q}(0)q(0)$. The result for the decay constant is

$$m_i^2F_i=\sqrt{2}\,\frac{n_C}{\pi^2}\left(\frac{1}{2m_i}\right)\int k^2dk\left[\frac{k}{E_u(k)}\right]^2\{\phi^+_{n\bar{n},N}(k)+\phi^-_{n\bar{n},N}(k)\}$$
$$+\frac{n_C}{\pi^2}\left(\frac{1}{2m_i}\right)\int k^2dk\left[\frac{k}{E_s(k)}\right]^2\{\phi^+_{s\bar{s},N}(k)+\phi^-_{s\bar{s},N}(k)\}. \tag{4.5}$$

[See Fig. 4(b).] The decay constant of Eq. (4.5) is dimensionless. For ease of comparison to the decay constants calculated for the a_0 mesons [3], it is useful to define a decay constant $f_i=(m_s^0-m_u^0)F_i$, where m_s^0 and m_u^0 are the current quark masses of the strange and up quarks. The factor of $(m_s^0-m_u^0)$ is introduced by Maltman so that the a_0 decay constants are similar in magnitude to the decay constants of the K_0^* mesons in the case that the a_0 and K_0^* mesons have similar wave functions [5,6]. We used $m_s^0-m_u^0=0.153$ GeV in our earlier work in order to make contact with Maltman's analysis, and we use that value here.

TABLE I. The first column shows the mass values obtained when solving the RPA equations with $G_{88}=10.02\,\mathrm{GeV}^{-2}$, $G_{00}=13.87\,\mathrm{GeV}^{-2}$, $G_{08}=0$, $\kappa=0.055\,\mathrm{GeV}^2$, $m_u=0.364\,\mathrm{GeV}$, and $m_s=0.565\,\mathrm{GeV}$. The second column presents the result including the effects of $K_S^{\pi\pi}(P^2)$, which were calculated in Ref. [2]. The third column shows $m_i^2F_i$ for each state, while the fourth column shows $m_i^2f_i$, with $f_i=(0.153\,\mathrm{GeV})F_i$.

$\tilde{m}$ (MeV) RPA	m (MeV) RPA plus dispersive effects	$m_i^2F_i$ (GeV^2)	$m_i^2f_i$ (GeV^3)
1004	950	0.472	0.0722
1502	1472	0.231	0.0353
1560	1540	0.327	0.0500
1835	1800	0.250	0.0383
1860	1850	0.214	0.0327
2059	2040	0.280	0.0428
2105		0.283	0.0433
2241		0.293	0.0448
2300		0.189	0.0285
2397		0.304	0.0465
2467		0.196	0.0300
2530		0.309	0.0473
2611		0.204	0.0312
2644		0.307	0.0470
2851		0.221	0.0338
3037		0.224	0.0343

V. NUMERICAL RESULTS

In this work we use $\mu=0.010\,\mathrm{GeV}$, $\kappa=0.055\,\mathrm{GeV}^2$, $m_u=0.364\,\mathrm{GeV}$, $m_s=0.565\,\mathrm{GeV}$, $G_{88}=10.02\,\mathrm{GeV}^{-2}$, $G_{00}=13.87\,\mathrm{GeV}^{-2}$, and $G_{08}=0$. The calculation of these parameters was described in the Introduction, so that our calculation of scalar meson properties is essentially parmeter-free. We find the lowest scalar-isoscalar state at 1004 MeV. (See Table I.) Dispersive effects due to the presence of $K_S(P^2)$ in the formalism move that energy down to 950 MeV, where the state may be identified with the $f_0(980)$. These dispersive effects and their role in shifting the calculated energies of the $q\bar{q}$ states is described in great detail in Ref. [2]. The calculation of $K_S(P^2)$ is rather complex. Some of the details are given in Ref. [14] where we studied the a_0 mesons. (There, the decay channels were $\pi\eta$, $K\bar{K}$, and $\pi\eta'$.) Since the calculations are covariant, the decay amplitudes, calculated at one-(quark-)loop order, may be calculated in any Lorentz frame. The amplitudes require regulation and the regulator is chosen so that reasonable widths, which are proportional to $\mathrm{Im}\,K_S(P^2)$, are obtained for the mesons considered. (We do not calculate final-state interactions when calculating the decay amplitudes. Some of the effects of such final-state interactions may serve to modify the value of the regulator chosen for the quark-loop integrals.)

In Table I we show the mass values obtained from the RPA equations in the first column. The second column shows

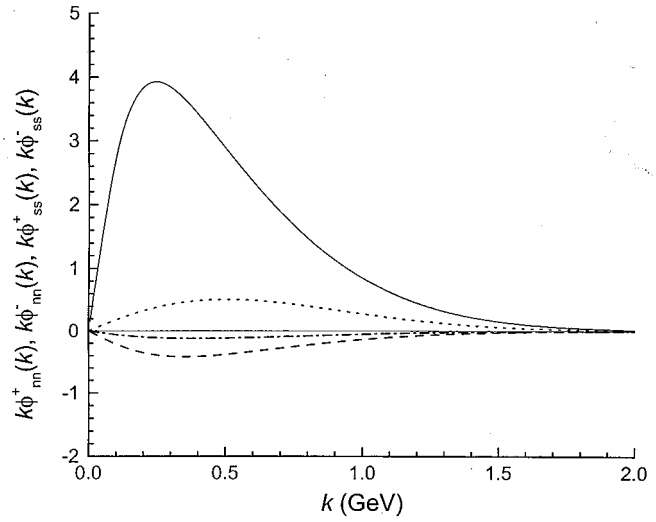

FIG. 5. The wave functions $k\phi^+_{n\bar{n}}(k)$ (solid line), $k\phi^-_{n\bar{n}}(k)$ (dotted line), $k\phi^+_{s\bar{s}}(k)$ (dashed line), and $k\phi^-_{s\bar{s}}(k)$ (dash-dotted line) are shown for the $1\ ^3P_0$ state that we identify with the $f_0(980)$ resonance. These wave functions correspond to the normalized wave functions introduced in Sec. III.

the values obtained when the effects of $K_S(P^2)$ are included [2]. Values of $K_S(P^2)$ calculated for the two-pion decay channel were given in Ref. [2]. There, they were denoted as $K^{\pi\pi}_{00}(P^2)$, $K^{\pi\pi}_{08}(P^2)$, and $K^{\pi\pi}_{88}(P^2)$. Since the $f_0(980)$ is mainly an $n\bar{n}$ state we may consider

$$K^{\pi\pi}_{n\bar{n}}(P^2)=\frac{K^{\pi\pi}_{88}(P^2)}{6}+\frac{\sqrt{2}}{3}K^{\pi\pi}_{08}(P^2)+\frac{K^{\pi\pi}_{00}(P^2)}{3}. \tag{5.1}$$

A typical value of $\mathrm{Im}\,K^{\pi\pi}_{n\bar{n}}(P^2)$ is 0.005 GeV^2 [2]. As we will

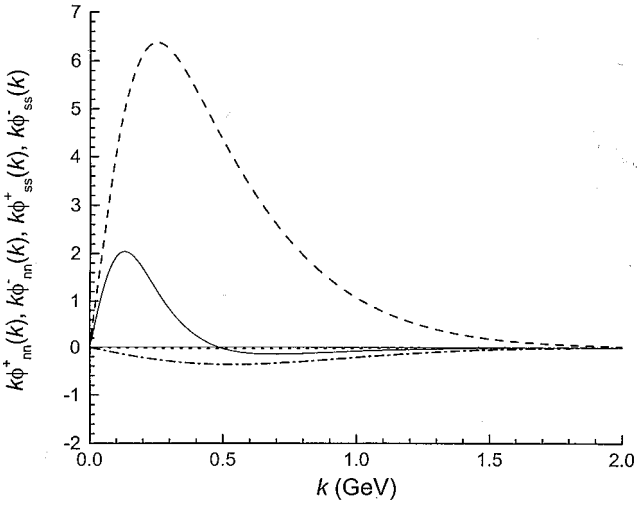

FIG. 6. The wave function for the $1\ ^3P_0$ state that we find at 1472 MeV. (See Table I.) After consideration of quarkonium-glueball mixing we would identify this state with the $f_0(1370)$.

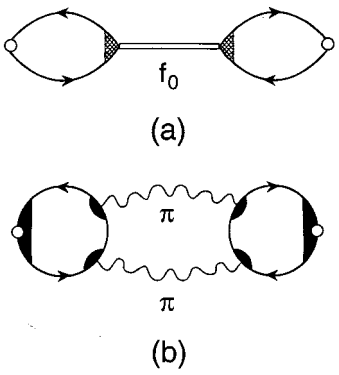

FIG. 7. (a) Contribution to the scalar-isoscalar correlation function due to the f_0 resonances. (b) Contribution to the scalar-isoscalar correlator that depends upon coupling to the two-pion continuum. (This contribution is quite small and may be neglected.)

see, the contribution of $\mathrm{Im}\,K^{\pi\pi}_{n\bar{n}}(P^2)$ to the imaginary part of the correlator introduced in Sec. VI is extremely small and may be neglected.

In Fig. 5 we show the normalized wave function amplitudes for the $1\ ^3P_0$ state that we identify with the $f_0(980)$. We see that that state is predominantly an $n\bar{n}$ state. In Fig. 6 we show the wave functions of the state at 1472 MeV. We see that that state is mainly of $s\bar{s}$ character. Some support for the assignment of that state to the $f_0(1370)$ is given in Sec. VII. However, the states at 1472 and 1540 MeV will mix with the scalar glueball which is believed to be at about 1.5–1.7 GeV.

VI. SCALAR-ISOSCALAR HADRONIC CORRELATION FUNCTION

In this work we study the hadronic correlator

$$C(P^2)=i\int d^4x\, e^{iP\cdot x}\langle 0|T(\bar{q}(x)q(x)\bar{q}(0)q(0))|0\rangle \tag{6.1}$$

and consider two contributions. These contributions are depicted in Fig. 7. In Fig. 7(a) we show the contribution of the f_0 resonances.

It is useful to separate the contribution of the $f_0(980)$ and write for the resonance contribution to $\mathrm{Im}\,C(P^2)$

$$\frac{1}{\pi}\mathrm{Im}\,C_R(P^2)$$
$$=m^4_{f_0(980)}f^2_{f_0(980)}\frac{1}{\pi}\frac{m_{f_{0(980)}}\Gamma_{f_{0(980)}}}{[P^2-m^2_{f_0(980)}]^2+m^2_{f_0(980)}\Gamma^2_{f_0(980)}}$$
$$+\sum_{i=2}^{16}m_i^4f_i^2\frac{1}{\pi}\frac{m_i\Gamma_i}{[P^2-m_i^2]^2+m_i^2\Gamma_i^2}, \tag{6.2}$$

where the sum is over the states shown in Table I. Here we choose $m_{f_0(980)}=0.980$ GeV, $\Gamma_{f_0(980)}=0.075$ GeV, and $\Gamma_i=0.200$ GeV. We remarked earlier that the contribution to

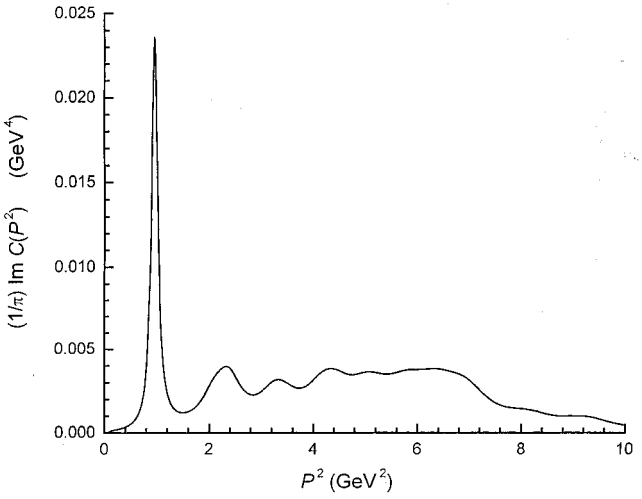

FIG. 8. Values of $(1/\pi)\mathrm{Im}\,C(P^2)$ are shown. Here, we use $m^2_{f_0(980)}f_{f_0(980)}=0.0722\ \mathrm{GeV}^3$, $\Gamma_{f_0(980)}=0.075$ GeV, and $m_{f_0(980)}=0.980$ GeV. For the other states we take $\Gamma=0.200$ GeV. The values of m_i and $m_i^2 f_i$ are given in Table I. [Note that $f_i=(0.153\ \mathrm{GeV})F_i$ for each state.] The values given in the figure may be compared to $(0.153\ \mathrm{GeV})^2\,\mathrm{Im}\,K^{\pi\pi}_{nn}(P^2)\simeq 1.2\times 10^{-4}$ GeV^4. Therefore, we see that the contribution from coupling to the two-pion continuum is negligible.

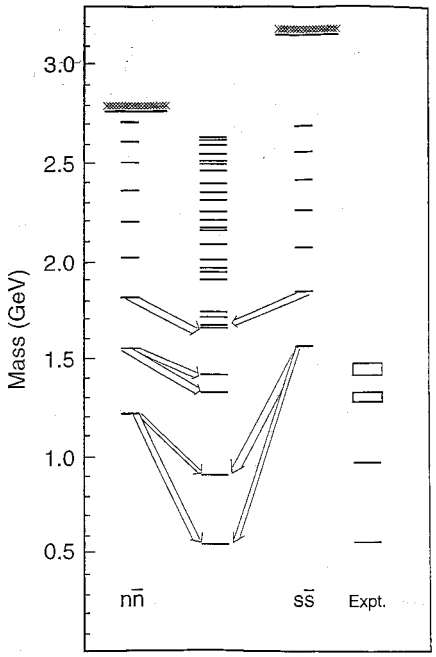

FIG. 9. The first and third columns of levels show the $n\bar{n}$ and $s\bar{s}$ states bound in the confining field, respectively. The second column shows the 28 levels found when the RPA Hamiltonian is brought to diagonal form [9]. The various arrows show the parentage of the resulting states. The $\eta(547)$ has 75% of the $1\ ^1S_0\ n\bar{n}$ state that has the γ_5 vertex and 25% of the $1\ ^1S_0\ s\bar{s}$ state that has the γ_5 vertex. These percentages are reversed for the $\eta'(958)$. The $1\ ^1S_0\ n\bar{n}$ and $s\bar{s}$ states with the $\gamma_0\gamma_5$ vertex are fragmented over many states. The $\eta(1295)$ and $\eta(1440)$ are almost entirely of $2\ ^1S_0\ n\bar{n}$ character. We have used $G_{88}=12.46\ \mathrm{GeV}^{-2}$, $G_{00}=8.60\ \mathrm{GeV}^{-2}$, and $G_V=12.46\ \mathrm{GeV}^{-2}$. The masses of the $\eta(547)$, $\eta'(958)$, $\eta(1295)$, and $\eta(1440)$ are found to be 550, 924, 1317, and 1411 MeV, respectively.

the correlator function arising from $K_S^{\pi\pi}(P^2)$ is very small, so that we take $\mathrm{Im}\,C(P^2)\simeq\mathrm{Im}\,C_R(P^2)$ in our analysis. Using the values given in Table I, we construct Fig. 8, which shows $(1/\pi)\mathrm{Im}\,C(P^2)$ for $P^2\leqslant 10\ \mathrm{GeV}^2$. The result is quite similar to that obtained for the scalar-isovector correlator described in Ref. [3].

VII. DISCUSSION

In this work we have used the parameters for G_S and G_D that yield a good fit to the energies of the $\eta(547)$, $\eta'(958)$, $\eta(1295)$, and $\eta(1440)$ [9]. (See Fig. 9.) Therefore, except for relatively small effects due to $K_S(P^2)$, the calculation reported here is parameter-free. It is found that the lowest f_0 state has a mass of approximately 1 GeV. There is no evidence in our calculations of the $f_0(400-1200)$ that now appears in the data tables. This matter is discussed in some detail in Ref. [15], where we define ''intrinsic'' and ''dynamically generated'' states. The intrinsic states are found by studying a $q\bar{q}\,T$ matrix [2] or by diagonalizing the RPA Hamiltonian, as was done in this work. Dynamical states appear when studying $\pi\pi$ scattering and these are not $q\bar{q}$ states. For example, t-channel and u-channel ρ exchange between the pions gives rise to a strong attraction that is responsible for the rapid increase with energy of the $L=0$, $I=0$ phase shift in the case of $\pi\pi$ scattering [15].

We have found that, if we wish to obtain a scalar state at 600 MeV, we have to increase G_S by about 50%, if we maintain the same value for G_D. That change represents a very large violation of the chiral symmetry of the Lagrangian and is unacceptable. [See Eq. (1.1).]

The lack of significant $\bar{q}q$ strength below the energy of the $f_0(980)$ resonance implies that the model of choice is the nonlinear sigma model rather than the linear model. However, the fact that an analysis of low-energy $\pi\pi$ scattering gives rise to a pole, which corresponds to a ''sigma meson'' of mass of about 500–600 MeV and a quite large width, has created a great deal of confusion [15]. For example, a study of $\pi\pi$ scattering in conjunction with the process $\pi\pi\rightarrow K\bar{K}$ led Surovtsev, Krupa, and Nagy to identify an $f_0(665)$ [16]. That result leads to their suggestion that one should consider a linear realization of chiral symmetry as appropriate. On the other hand, Li, Zou, and Li [17] have also studied $\pi\pi$ scattering and have come to a different conclusion. They show that t- and u-channel ρ exchange gives rise to a pole at $(0.36-0.53i)$ GeV. [They also introduce an additional state with a pole at $(1.67-0.26i)$ GeV to increase the phase shift obtained from ρ exchange, so as to fit the $\pi\pi$ S-wave amplitude.] The authors of Ref. [17] conclude that there is no state of $q\bar{q}$ character below 1 GeV. We have come to the same conclusion using somewhat different arguments [15]. While we have also studied the role of ρ exchange as it pertains to the S-wave phase shift [15], we have seen in the work reported here that a calculation of scalar-isoscalar $q\bar{q}$ states does not produce a low-mass sigma.

Another recent work of interest is that of Ref. [18]. There, the authors obtain a σ meson of mass 630 MeV at zero temperature and density and use the ratio of the σ mass to the π mass to provide a quantitative signal for chiral symmetry restoration at finite temperature and density. However, these authors identify the σ of their model with the σ seen in $\pi\pi$ scattering. It appears clear to us that the σ obtained from the study of $\pi\pi$ scattering is not the chiral partner of the pion [19].

The authors of both Refs. [16] and [17] find a quite small width for the two-pion decay of the $f_0(1370)$. That can be explained in our model, since the state we tentatively identify with the $f_0(1370)$ is mainly of $s\bar{s}$ character. However, the $f_0(1370)$ decays predominantly to the four-pion channel. That suggests that the $f_0(1370)$ may have a large scalar glueball component. The entire matter of quarkonium-glueball mixing in the scalar-isoscalar states deserves further investigation.

We have noted in this work that the nature of the various scalar states that appear in the data tables is a matter of some controversy. Various models and configuration assignments are described in Refs. [19–29]. We believe our work has introduced an important element in the attempt to resolve these issues.

While the nature of the $f_0(400-1200)$ [or $\sigma(500-600)$] is a matter of some controversy, the nature of the $f_0(980)$ is also subject to various interpretations. One approach regards the $f_0(980)$ as a four-quark bound state [30] and another as a $K\bar{K}$ ''molecule'' [31]. It was early thought that the $f_0(980)$ might be a glueball [32]. Recently the $f_0(980)$ has been seen in neutrino-nucleus charged current interactions, where it is found that the $f_0(980)$ behaves as an ordinary $q\bar{q}$ state. The authors of Ref. [33] also remark that ''All measured characteristics of $f_0(980)$ production in Z^0 decays are consistent with the $f_0(980)$ being a conventional scalar meson.''

Finally, we note that confinement is quite a small effect when calculations are made for the $\pi(138)$ and $K(495)$ mesons. It may be best to neglect confinement for these Goldstone bosons, or to perform calculations in Euclidean space, to ensure that the relations that follow from the chiral symmetry of the Lagrangian are preserved [12].

APPENDIX

In this Appendix we provide values for $\overline{H}_{n\bar{n}}(k,k')$, $\overline{H}_{s\bar{s}}(k,k')$, and $\overline{V}_C(k,k')$:

$$\overline{H}_{n\bar{n}}(k,k') = -\frac{2}{\pi^2} n_C \frac{k^2 k'^2}{E_n(k)E_n(k')} e^{-k^2/2\alpha^2} e^{-k'^2/2\alpha^2}, \tag{A1}$$

$$\overline{H}_{s\bar{s}}(k,k') = -\frac{2}{\pi^2} n_C \frac{k^2 k'^2}{E_s(k)E_s(k')} e^{-k^2/2\alpha^2} e^{-k'^2/2\alpha^2}, \tag{A2}$$

$$\overline{V}^C_{n\bar{n}}(k,k') = \frac{1}{(2\pi)^2} \frac{kk'}{E_n(k)E_n(k')} [2kk' V_0^C(k,k') + m_u^2 V_1^C(k,k')], \tag{A3}$$

and

$$\overline{V}^C_{s\bar{s}}(k,k') = \frac{1}{(2\pi)^2} \frac{kk'}{E_s(k)E_s(k')} [2kk' V_0^C(k,k') + m_s^2 V_1^C(k,k')] \tag{A4}$$

with

$$V_l(k,k') = \frac{1}{2} \int_{-1}^{1} dx\, P_l(x) V^C(\vec{k}-\vec{k}'), \tag{A5}$$

etc.

[1] L. S. Celenza, Bo Huang, Huangsheng Wang, and C. M. Shakin, Phys. Rev. C **60**, 025202 (1999); **60**, 039901(E) (1999).

[2] L. S. Celenza, Shun-Fun Gao, Bo Huang, Huangsheng Wang, and C. M. Shakin, Phys. Rev. C **61**, 035201 (2000).

[3] C. M. Shakin and Huangsheng Wang, Phys. Rev. D **63**, 114007 (2001).

[4] C. M. Shakin and Huangsheng Wang, Phys. Rev. D **63**, 074017 (2001).

[5] K. Maltman, Phys. Lett. B **462**, 14 (1999).

[6] K. Maltman, ''Scalar Decay Constants and the Nature of the $a_0(980)$,'' presented at the International Conference on Quark Nuclear Physics, Adelaide, 2000, hep-ph/0005155.

[7] L. S. Celenza, Huangsheng Wang, and C. M. Shakin, Phys. Rev. C **63**, 025209 (2001).

[8] T. Hatsuda and T. Kunihiro, Phys. Rep. **247**, 221 (1994).

[9] C. M. Shakin and Huangsheng Wang, Brooklyn College Report No. BCCNT 01/061/304, 2000. In this work we used $G_{88}^P = 12.46$ GeV^{-2} and $G_{00}^P = 9.10$ GeV^{-2}; however, use of $G_{00}^P = 8.60$ GeV^{-2} leads to a better fit to the spectrum.

[10] A. L. Fetter and J. D. Walecka, *Quantum Theory of Many-Particle Systems* (McGraw-Hill, New York, 1971).

[11] Bo Huang, Xiang-Dong Li, and C. M. Shakin, Phys. Rev. C **58**, 3648 (1998).

[12] L. S. Celenza, Xiang-Dong Li, and C. M. Shakin, Phys. Rev. C **55**, 1492 (1997).

[13] A. P. Szczpaniak and E. B. Swanson, Phys. Rev. D **55**, 3987 (1997).

[14] L. S. Celenza, Bo Huang, Huangsheng Wang, and C. M. Shakin, Phys. Rev. C **60**, 065210 (1999).

[15] C. M. Shakin and Huangsheng Wang, Phys. Rev. D **63**, 014019 (2001).

[16] Y. S. Surovtsev, D. Krupa, and M. Nagy, Phys. Rev. D **63**, 054024 (2001).

[17] Long Li, Bing-Song Zou, and Guang-Lie Li, Phys. Rev. D **63**, 074003 (2001).

[18] A. Barducci, R. Casalbuoni, G. Pettini, and R. Gatto, Phys. Rev. D **63**, 074002 (2001).

[19] Ulf-G. Meissner, contribution to the III Workshop on Physics and Detectors for DAΦNE, Frascati, 1999, hep-ph/0001066.
[20] M. R. Pennington, ''Riddle of the Scalars: Where Is the σ?'', talk presented at the Workshop on Hadron Spectroscopy (WHS99), Frascati, 1999, hep-ph/9905241.
[21] T. Hannah, Phys. Rev. D **60**, 017502 (1999).
[22] T. Kunihiro and T. Hatsuda, Phys. Lett. B **240**, 209 (1990).
[23] T. Kunihiro, invited talk presented at the Workshop on Hadron Spectroscopy (WHS99), Frascati, 1999, hep-ph/9905262.
[24] D. Black, A. H. Fariborz, and J. Schechter, Phys. Rev. D **61**, 074001 (2000).
[25] D. Black, A. H. Fariborz, F. Sannino, and J. Schechter, Phys. Rev. D **59**, 074026 (1999).
[26] N. A. Törnqvist, Z. Phys. C **68**, 647 (1995); N. A. Törnqvist and M. Roos, Phys. Rev. Lett. **76**, 1575 (1996).
[27] S. Ishida *et al.*, Prog. Theor. Phys. **95**, 745 (1996); **98**, 1005 (1997).
[28] M. K. Volkov and V. L. Yudichev, Int. J. Mod. Phys. A **14**, 4621 (1999).
[29] M. K. Volkov and V. L. Yudichev, Eur. Phys. J. A **10**, 109 (2001); **10**, 223 (2001).
[30] R. L. Jaffe and K. Johnson, Phys. Lett. **60B**, 201 (1976); R. L. Jaffe, Phys. Rev. D **15**, 267 (1977); **15**, 281 (1977).
[31] J. Weinstein and N. Isgur, Phys. Rev. D **41**, 2236 (1990).
[32] D. Robson, Nucl. Phys. **B130**, 328 (1977).
[33] NOMAD Collaboration, P. Astier *et al.*, Report No. CERN-EP/2001-024, 2001.